Landslides (2021) 18:2907–2921
DOI 10.1007/s10346-021-01701-w
Received: 23 January 2021
Accepted: 13 May 2021
Published online: 21 May 2021

Xiaoyu Yi · Wenkai Feng · Huilin Bai · He Shen · Haobin Li

Catastrophic landslide triggered by persistent rainfall in Sichuan, China: August 21, 2020, Zhonghaicun landslide

Abstract At approximately 3:50 a.m. (UTC + 8) on August 21, 2020, a massive rainfall-induced landslide occurred in Zhonghaicun, Fuquan town, Hanyuan County, Sichuan Province, China, forming an approximately 40.85 × 10^4 m^3 landslide accumulation, burying eight houses and approximately 100 m of roads, and causing long-term traffic interruptions. The landslide was comprehensively evaluated through field investigation, UAV photography, borehole drilling, and laboratory tests. According to movement and accumulation characteristics, the landslide is divided into the main sliding zones (the source area, impact sliding area, shoveling-accumulation area, and accumulation area) and landslide-affected zones. The deformation and failure of the Zhonghaicun landslide are related to the lithology (existence of a weak interlayer), geomorphology (microrelief changes), and antecedent rainfall. However, the main trigger of the landslide is continuous rainfall, which increases the landslide saturation and pore water pressure and reduces the mechanical strength of the weak layer. The landslide failure mode is complex. The upper slope is affected by rainfall and loses stability first. Under the impact of the sliding mass, sliding of the lower slope is triggered. This study of the Zhonghaicun landslide characterizes the evolution process of a complex rainfall-induced landslide and provides ways to mitigate landslide disasters.

Keywords Rainfall · Xigeda Formation · Landslide characteristics · Evolution process · Xiaoyu Yi is the first author.

Introduction

Landslides are a common geological disaster and occur widely globally. The occurrence of landslides depends on many factors closely related to local conditions (such as topography, geological structure, and lithology), meteorological and hydrological conditions, and geophysical processes. Landslides can be triggered by rainfall (Fan et al. 2017a; Li et al. 2019), reservoir water (Yin et al. 2010; Tang et al. 2019), flood (Bhardwaj et al. 2019; Bezak et al. 2020), ice melting (Kotlyakov et al. 2004), earthquake (Yin et al. 2011; Shrestha and Kang 2019), and human engineering activities (Zhang et al. 2012; Ma et al. 2019a), and sometimes a combination of the above factors (Fan et al. 2017b; Yu et al. 2020). Previous studies show that rainfall is the most active and changeable natural factor among many variables and is one of the main factors inducing landslides (Emanuel 2005; Guzzetti et al. 2007).

In August 2020, continuous heavy rainfall occurred in Hanyuan County, Sichuan Province, China. At approximately 3:50 a.m. on August 21, 2020 (UTC + 8), a large-scale landslide occurred in Zhonghaicun, Fuquan town, Hanyuan County, following several days of rainfall (N29°20′30″, E102°41′39″) (He et al. 2020). The landslide broke away from the slope at an average elevation of 1030 m and started sliding. Along its path, the landslide hit and scraped the loose deposits on the initial slope until its front edge moved to the Liusha River at an elevation of 850 m, and the landslide stopped moving when contiguous houses blocked it. The landslide damaged eight houses and caused traffic disruption on the S435 highway (Fig. 1). Although the local government took evacuation measures before the landslide, due to the lack of understanding of the disaster mechanism and management negligence, the landslide disaster still caused seven deaths, and two people went missing.

After the landslide, the Sichuan Provincial People's Government immediately launched a rescue operation. To explore the causes of this catastrophic landslide, researchers arrived at the landslide disaster site on August 23. They conducted a comprehensive study through field investigation, unmanned aerial vehicle (UAV) photography, and laboratory tests after completing on-site emergency rescue work. The drilling data and monitoring data after the landslide were also analyzed in detail. Based on the above work, the characteristics and failure mechanism of the Zhonghaicun landslide were analyzed. The case study in this paper provides ideas for the in-depth study of complex landslides induced by rainfall. The information provided in this paper can help to prevent and reduce the casualties and property losses caused by landslides in Southwest China.

Geological settings

The study area is located in Fuquan town, Hanyuan County, Sichuan Province, on the left bank slope of the Liusha River, a tributary of the Dadu River, 310 km away from Chengdu, the capital of Sichuan Province (Fig. 2). Hanyuan County has a subtropical monsoon climate with an annual average temperature of 18.0 °C. The observational rainfall data from the local rain gauge (Fig. 2) are shown in Fig. 3. Beginning on August 7, the region experienced many heavy rainfall events. Before the landslide, the cumulative precipitation in August was 266.1 mm, 104.8 mm more than the highest value of 161.3 mm (June) from May to July in the same year, and 124.6 mm more than the average value of the same period in previous years. The antecedent rainfall at that time could have played a vital role in landslide damage.

The landslide is located in low- to middle-elevation mountains with a slope dipping north at an average angle of 16°. Four levels of gentle slope platforms are developed in the landslide area, forming topography with alternating steep and gentle slopes (Fig. 4). The highest elevation of the landslide source area is approximately 1030 m, and the landslide toe is located on the left bank of the Liusha River, at approximately 850 m, with a relative height difference of 180 m. All these features provide favorable geomorphic conditions for slope instability.

According to the field investigation, borehole data, and a 1:200000 geological map (Geological Bureau of Sichuan Province, 1971), the lithology of the landslide primarily consists of the overlying Quaternary-Holocene accumulation of eluvium silty clay

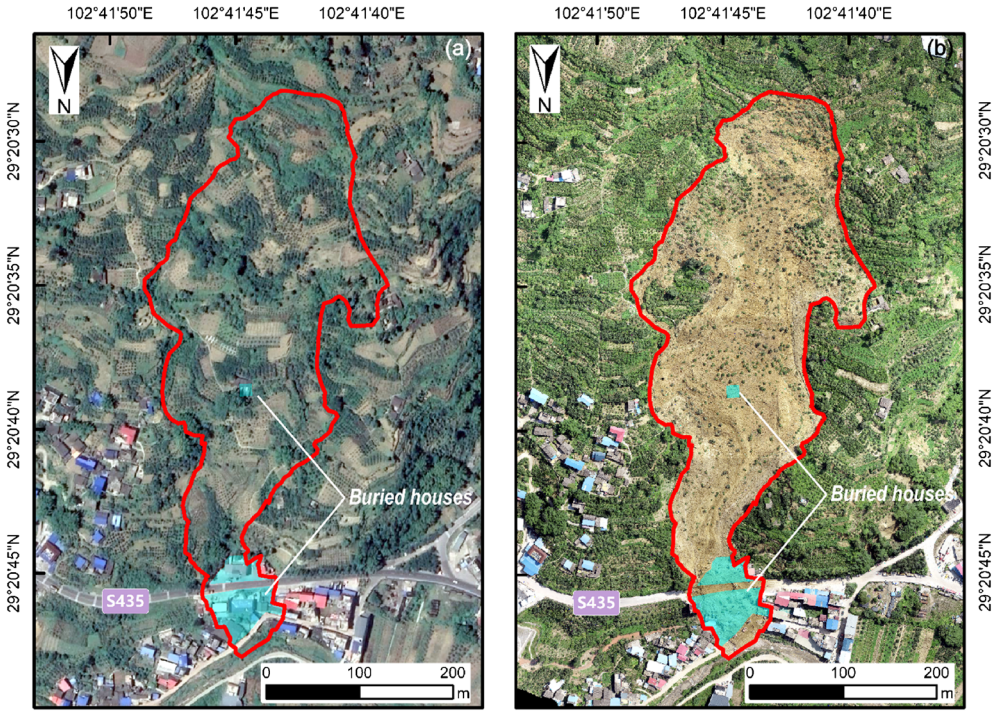

Fig. 1 Images of Zhonghaicun before and after the landslide: **a** Google Earth image before the landslide (May 14, 2018); **b** digital orthophoto map (DOM) from the unmanned aerial vehicle (UAV) after the landslide (August 21, 2020)

(Q_4^{el+dl}) and the underlying bedrock of the Neogene-Quaternary Xigeda Formation (NQx). The eluvial and slope silty clay is approximately 0.5–4.0 m thick, yellowish-brown, and loose, and the gravel content is generally 10–25%. The Xigeda Formation is mainly grayish-yellow siltstone intercalated with thin claystone and carbonaceous claystone. Due to the short diagenetic time, the completely weathered stratum in the Xigeda Formation is 5–20 m thick and has a loose structure similar to soil.

Deformation history

In August 2020, the rainfall in Hanyuan County was higher than that in previous years (Fig. 3). On August 19, 2020, local observers

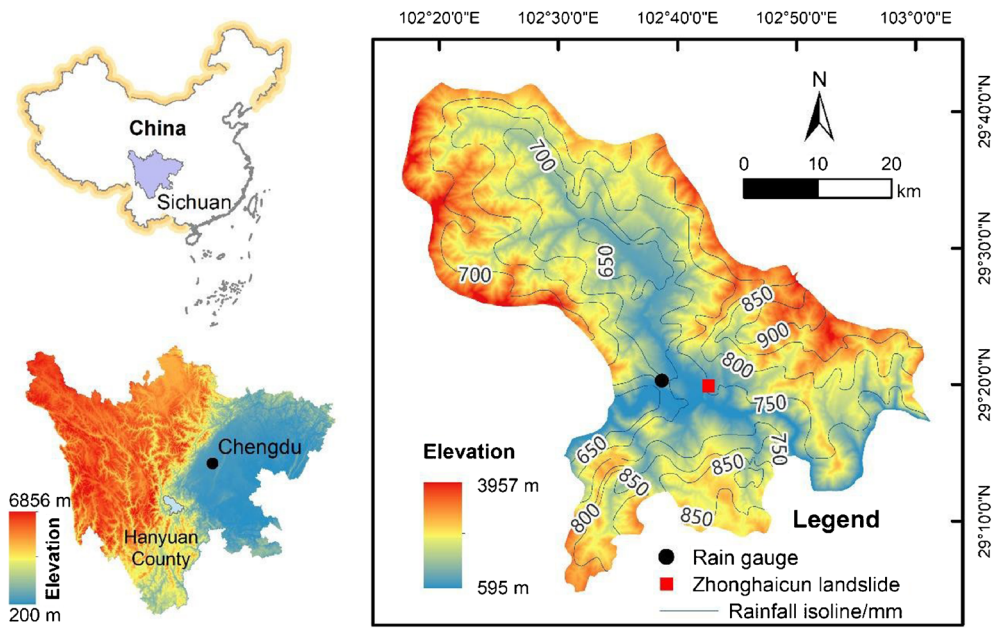

Fig. 2 The Zhonghaicun landslide and rain gauge location

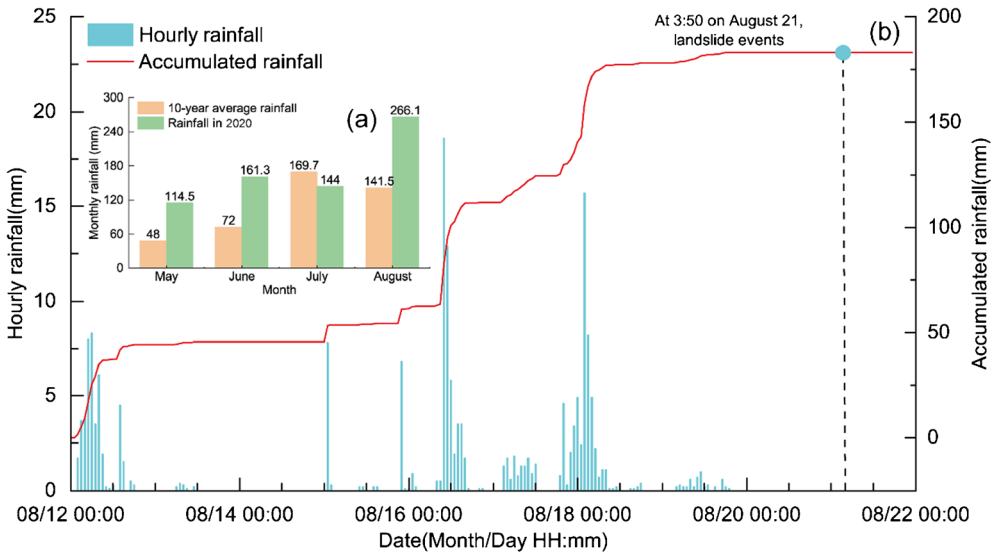

Fig. 3 Daily rainfall and monthly cumulative rainfall recorded by rain gauges near the Zhonghaicun landslide

found several tensile cracks in the landslide's rear crown (Fig. 5a, b, c, e, and h), with an extension length of approximately 2.0–8.0 m and dislocation depth of 5.0–30.0 cm. On the morning of August 20, 2020, observers discovered a new tensile crack at the crown of the landslide (Fig. 5d), with an extension length of approximately 8.0 m and a dislocation depth of 2.0 m. Additionally, the observers found an increase in the extension length and width of the crack shown in Fig. 5e, with a dislocation depth of 2.5 m (Fig. 5d). In the afternoon on August 20, 2020, to avoid the possibility of heavy casualties from the landslide, the Fuquan town government organized to evacuate 55 residents from 14 nearby households. On August 21, 2020, at approximately 3:50 a.m., a landslide occurred (Fig. 5e and h), and nearby residents heard a violent sound and felt the ground shaking. The process lasted for approximately 1 min. Unfortunately, some residents did not comply with the evacuation regulations and returned to their homes without permission, so the landslide caused casualties.

Characteristics of the landslide

The highest elevation of the Zhonghaicun landslide crown is 1030 m, and the lowest elevation of the landslide toe is 850 m. Affected by the terrain on the landslide path, the sliding direction changes from 25 ° to 355 °, and the final accumulation shape is irregular. According to the elevation change and geomorphic characteristics of the Zhonghaicun landslide, the main sliding zones and the landslide-affected zones can be distinguished (Fig. 6). The former can be divided into the source area (*Zone A*), impact sliding area (*Zone B*), shoveling-accumulation area (*Zone C*), and accumulation area (*Zone D*). There are three landslide-affected zones: one is the traction deformation area (*Zone I*) affected by the source area (*Zone A*), and the other two are the impact-traction deformation areas (*Zone II-1* and *Zone II-2*) affected by the source area (*Zone A*) and impact sliding area (*Zone B*), which are located on both sides of *Zone B*.

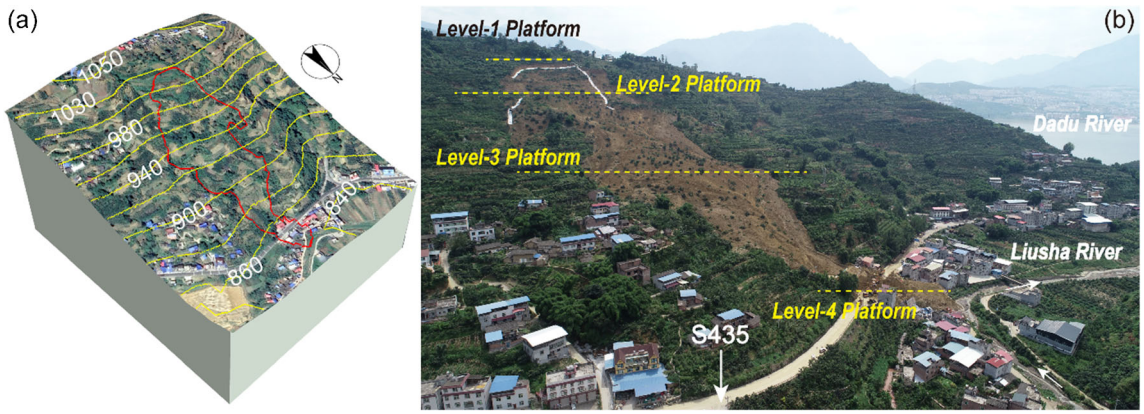

Fig. 4 Three-dimensional topographic maps of the landslide area

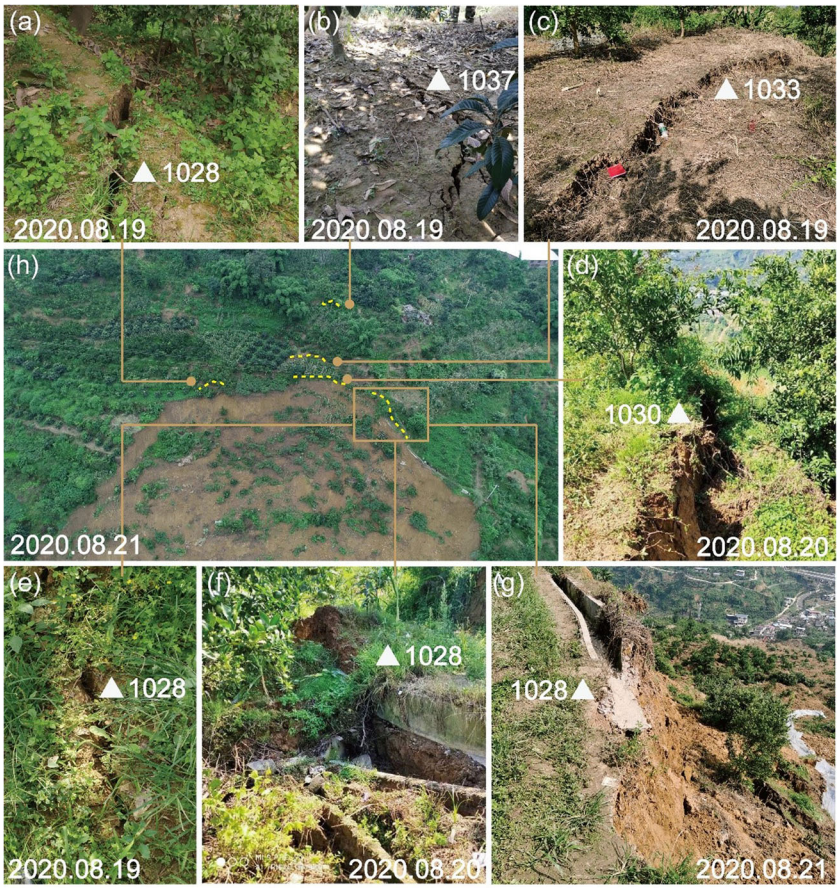

Fig. 5 Tensile cracks in the crown of the Zhonghaicun landslide photographed by inspectors, with the location, elevation, deformation value, and photo time of the crack marked on the image. **a**–**f** Tensile cracks before the landslide; **e**–**g** photos of tensile cracks at the same location at different times; **f** UAV image of the rear crown of the Zhonghaicun landslide, with the location and elevation of the crack marked

Major sliding zones

Source area (Zone A)

The source area (*Zone A*) is between 990 and 1030 m, with a relative elevation difference of 40 m (Fig. 7a). The source area is 65–140 m wide and 100 m long, and the deposit area is approximately 1.2×10^4 m^2. According to the drilling data, the sliding surface depth is approximately 15.0–27.5 m, and the landslide volume of the source area (*Zone A*) is 27.0×10^4 m^3.

The upper part of the source area is the level-1 gentle slope platform, and the crown and the boundary on both sides of the source area form a 'round-backed armchair' landform (Fig. 7a, b, and c). The height of the main scarp is approximately 5–14 m, and the slope is approximately 60°–80° (Fig. 7d). The sliding scratches on the sliding zone are clear, and the direction of the scratches is consistent with the sliding direction (Fig. 7e). Due to the source area's instability, most of the sliding material (~ 18×10^4 m^3) moved downward and accumulates in the middle and lower parts of the slope, and some of the sliding material (~ 9.0×10^4 m^3) remained in the middle and lower parts of the source area (Fig. 7a).

After the landslide, an inclinometer was installed in the Z01 drill hole in the source area (Figs.6b and 7a). The displacement data show that a new sliding surface is gradually formed at 9.5 m, and the maximum displacement was 4.5 cm (Fig. 8). In the future, rainfall may cause the landslide deposits of the source area to slide.

Impact sliding area (Zone B)

The impact sliding area (*Zone B*) is located below the source area (*Zone A*) at elevations of 940–990 m. The plane shape is approximately zonal, and the area is approximately 1.5×10^4 m^2 (Fig. 9a). Before the landslide, the upper part of the area was a level-2 platform with a slope of approximately 10°. Under the impact load of loose accumulation in the source area (*Zone A*), sliding failure occurred in the impact sliding area (*Zone B*). After the failure of the impact sliding area (*Zone B*), a landslide scarp (Fig. 9b and c) with an elevation difference of 7–14 m was formed on both sides. During the field investigation, a residual sliding zone was found near the right scarp. After removing the clay with a high gravel content on the surface, a smooth mudded sliding zone with a thickness of approximately 2 cm can be seen (Fig. 9d).

Shoveling-accumulation area (Zone C)

The shoveling-accumulation area (*Zone C*) ranges from 940 to 870 m, with an elevation difference of approximately 70 m and an area of approximately 3.20×10^4 m^2 (Fig. 10a). The upper part of the shoveling-accumulation area (*Zone C*) is the level-3 platform with

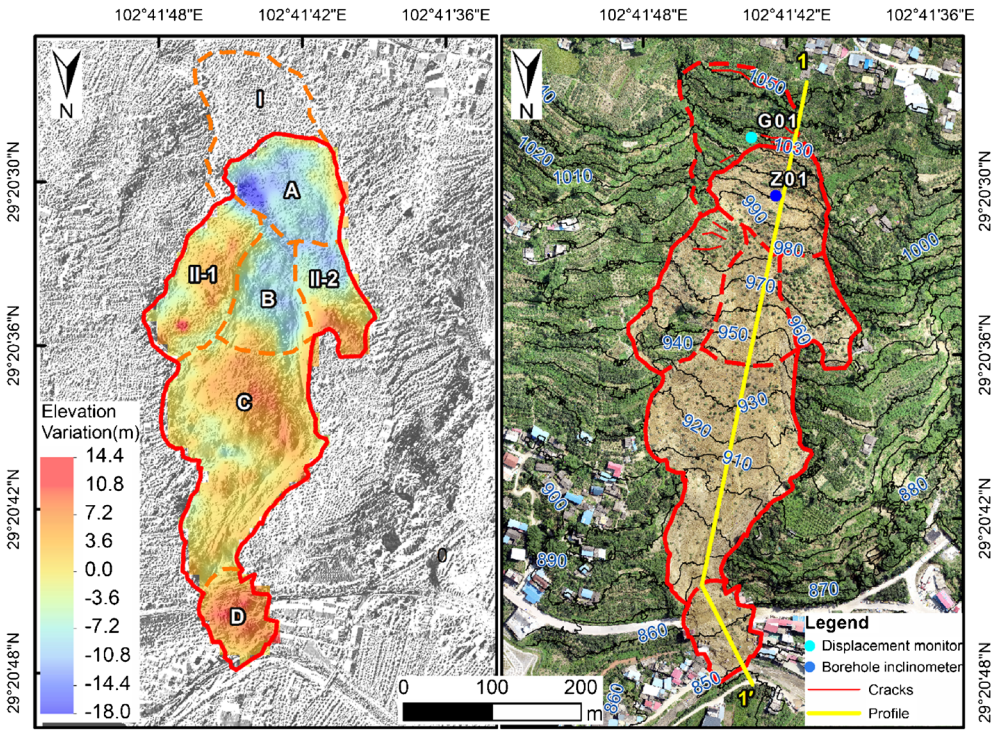

Fig. 6 Post-landslide topography: **a** post-landslide digital surface model (DSM) and elevation difference; **b** post-landslide DOM. In (**a**), A–D mark the zone of major sliding, I–II are different areas affected by instabilities; the displacement monitor and borehole inclinometer arrangement post-landslide are shown in (**b**)

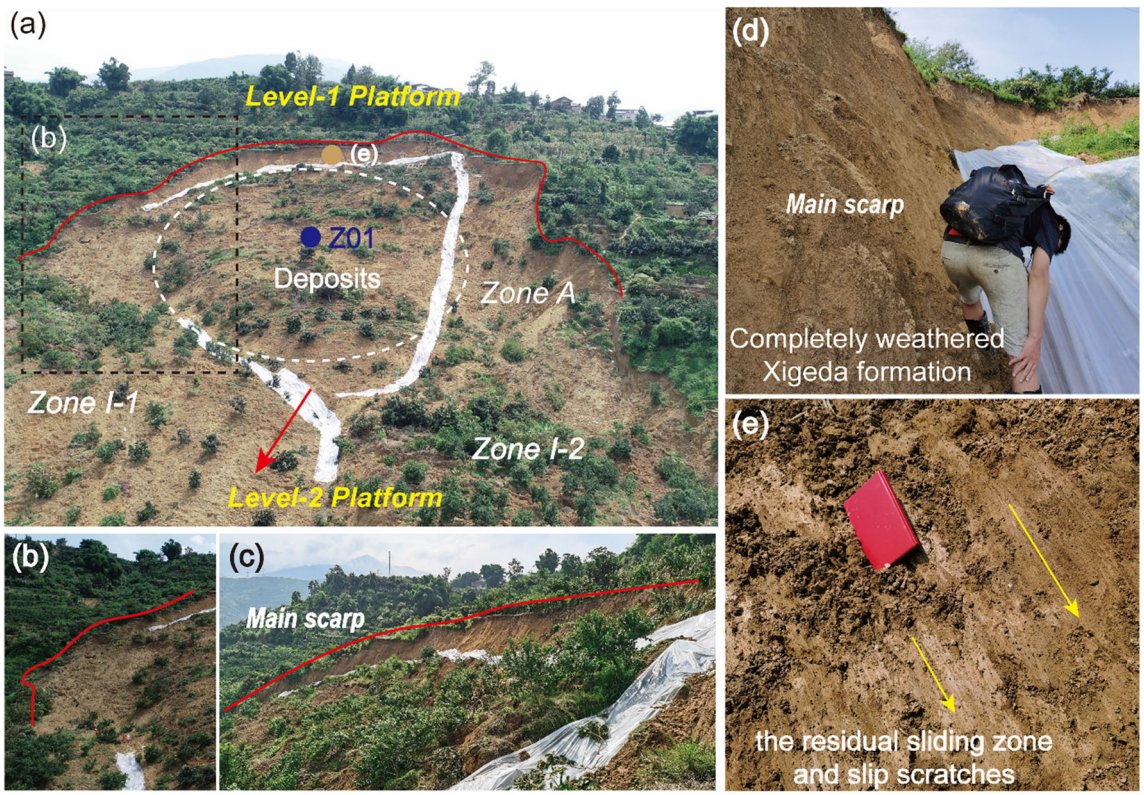

Fig. 7 Photos of the source area (*Zone A*) of the Zhonghaicun landslide: **a** an overview of the source area (*Zone A*); **b**–**c** the main scarp of the Zhonghaicun landslide; **d** the main scarp with completely weathered Xigeda Formation; **e** the residual sliding zone and slip scratches

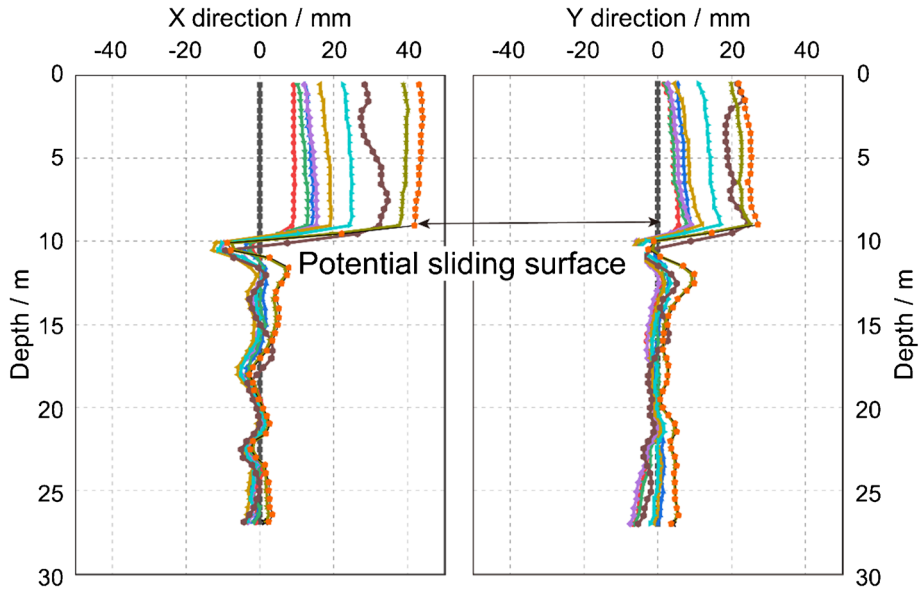

Fig. 8 The displacement results monitored by inclinometer Z01. The locations of the inclinometers are listed in Fig. 7b, and monitoring occurred from September 10, 2020, to September 30, 2020

a slope of approximately 8°–12°, and much landslide debris accumulated on the level-3 platform (Fig. 10b). There are multistage scarps, with slopes of approximately 10°–20° in the lower part of the shoveling-accumulation area (*Zone C*). To release its energy, the high-speed debris flow sliding along the terrain continuously scraped the original residual layer of the slope, which led to an increase in the volume of the debris flow. Due to the influence of steep and gentle slope changes and the disintegration of loose deposits, the scraping effect was weakened, the flow area was gradually narrowed, with its width being reduced from 215 to 75

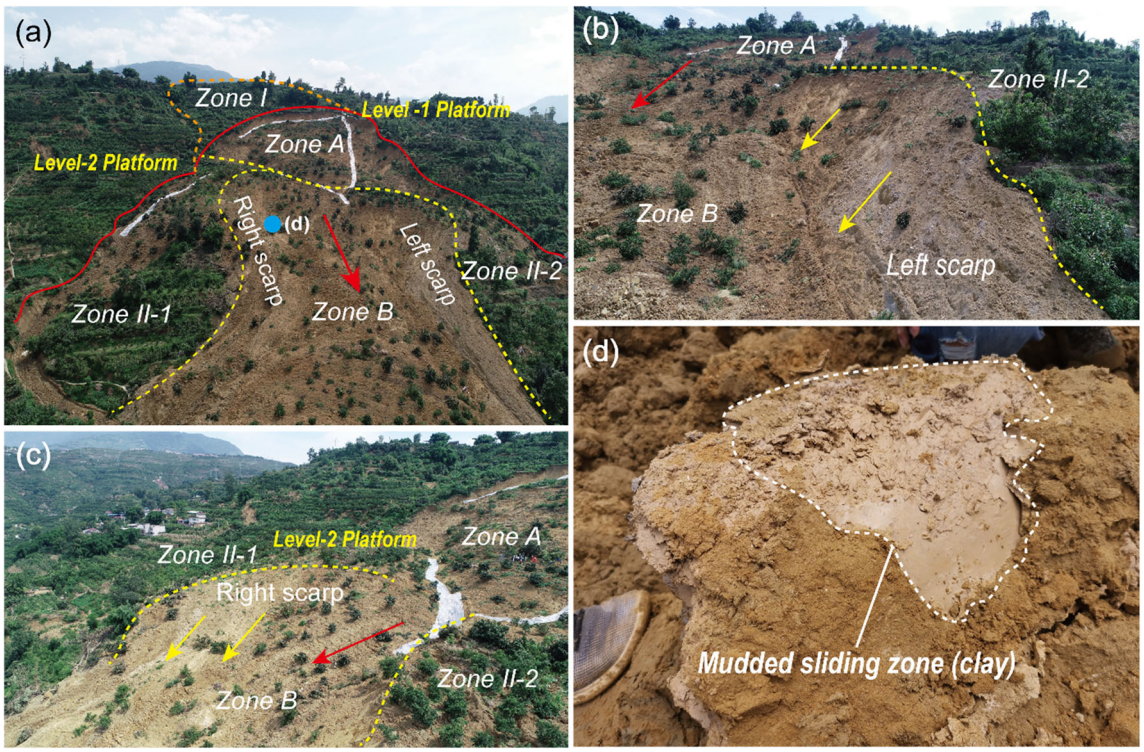

Fig. 9 Photos of the impact sliding area (*Zone B*) of the Zhonghaicun landslide: **a** an aerial view of the source area; **b**–**c** the left and right scarps of the Zhonghaicun landslide; **d** the mudded sliding zone in the impact sliding area

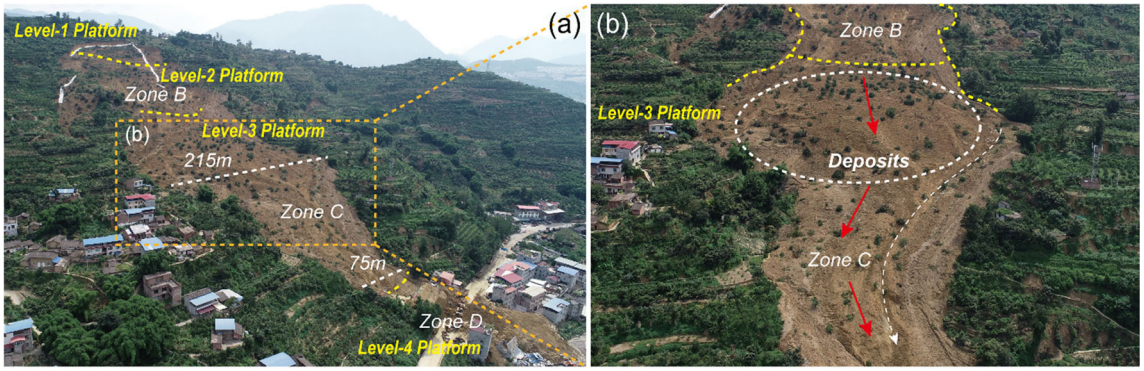

Fig. 10 The shoveling-accumulation area (*Zone C*) of the Zhonghaicun landslide: **a** the landslide deposits remaining in the shoveling-accumulation area; **b** the width and movement direction of debris flow change due to topography

m (Fig. 10a), and the sliding direction was deflected from 25° to 355° (Fig. 10b).

Accumulation area (Zone D)

The accumulation area (*Zone D*) is between 870 and 850 m, with an elevation difference of approximately 20 m and an area of approximately 0.82 × 10^4 m^2 (Fig. 11a and b), and the S435 highway crosses it. The main residential area before the landslide is shown in Fig. 1a. When the landslide occurs, the debris flow is controlled by the terrain and washed down the slope. Finally, the landslide stopped moving after being blocked by houses and accumulated on the left bank of the Liusha River (Fig. 11b and c). During the field investigation on August 23, water seepage phenomena were found after excavation in the accumulated mass at the slope toe (Fig. 11d).

Landslide-affected zones

Traction deformation area (Zone I)

The traction deformation area (*Zone I*) is located in the upper part of the source area (*Zone A*), between 1050 and1030 m, with a slope of approximately 20° and an area of approximately 2.65 × 10^4 m^3. After the landslide, the main scarp was formed in the crown, and

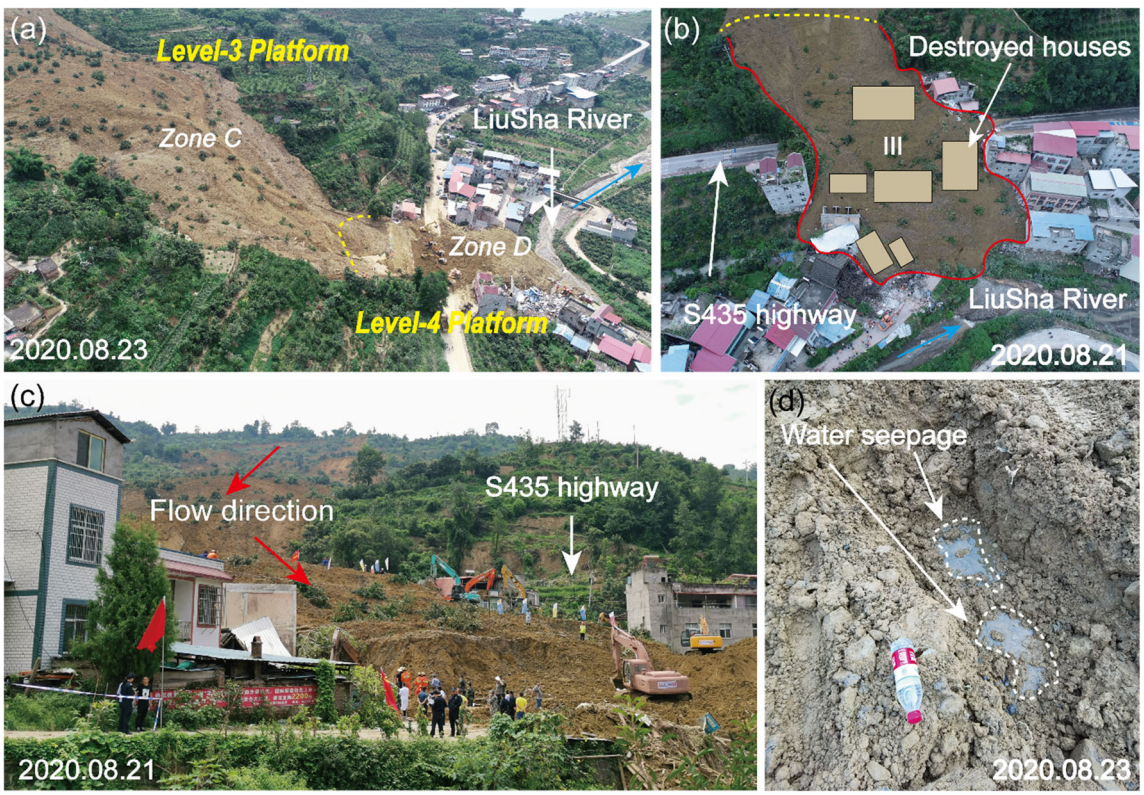

Fig. 11 The accumulation area (*Zone D*) of the Zhonghaicun landslide: **a** geomorphological characteristics of the front part of the Zhonghaicun landslide; **b** many buried houses in the landslide accumulation area; **c** debris flow material in the toe/accumulation zone; **d** water seepage in debris flow at the slope toe

Table 1 Tensile cracks in the traction deformation area

Crack number	Altitude (m)	Strike angle (°)	Extension length (m)	Maximum width (cm)
C1	1050	110	100	20
C2	1036	120	55	10
C3	1032	100	60	10
C4	1030	90	10	10
C5	1015	90	5	2

the free face and gravity promoted the appearance of traction deformation and many tensile cracks in the traction deformation area (*Zone I*) (Table 1). The strike of the tensile cracks is 90° to 120° and is roughly parallel to the main scarp of the landslide. The length of the largest crack reaches 100 m, extending in an arc.

After the landslide, global navigation satellite system (GNSS) surface displacement monitoring station G01 (Fig. 7b) was installed in the traction deformation area (*Zone I*). From August 25, 2020, to September 23, 2020, the cumulative horizontal displacement of G01 was 37.5 mm, the cumulative vertical displacement was 22.3 mm, and the combined displacement was 43.63 mm (Fig. 12). The monitoring data show that the initial deformation rate was higher due to slope stress adjustment after the landslide. After some time, the deformation rate tended to stabilize and enter the stage of constant velocity deformation, and the overall sliding failure seems unlikely. However, there were many tension cracks in the slope, which were conducive to rainfall infiltration. A rainfall intensity lower than the current rainfall intensity may cause instability in the region in the future.

Impact-traction deformation area (Zone II)

The impact-traction deformation areas (*Zone II-1* and *Zone II-2*) are located on both sides of the impact sliding area (*Zone B*). Before sliding, there is a microrelief of a small gully (Figs. 6, 7a, and 9a). The impact-traction deformation area (*Zone II*) was mainly affected by the impact of the sliding mass in the source area (*Zone A*), and the traction caused by the failure of the impact sliding area (*Zone B*) also affected the deformation of the slope. In the field investigation, multiple cracks (Fig. 7b and Table 2) were found on the slope of *Zone II-1*; these cracks were mainly distributed on the level-2 platform near the source area (*Zone A*) and had strike angles of 70°–110°, which were parallel to the main scarp of the source area (*Zone A*). Due to blocking by the level-2 platform, the impact of landslide material on the lower part of *Zone II-1* was low, and the original vegetation of the slope was not affected (Fig. 13a and b). Since the west side of the level-2 platform of the initial slope was lower than the east side, the platform in the *Zone II-2* area close to the source area (*Zone A*) was affected by the impact and traction, resulting in greater deformation than that in *Zone II-1*. The left boundary formed a scarp of 1–3 m (Fig. 13c), and some debris was deposited on the slope below the platform (Fig. 13d).

Based on the elevation change before and after sliding, the landslide area is 8.12×10^4 m^2, and the volume of the main accumulation area is 25.56×10^4 m^3. Considering the entrainment and scraping effect of the landslide, the volume of the landslide will further increase; assuming that the volume of the broken mass increases by approximately 25% (Geertsema et al. 2006; Xu et al. 2016; Ma et al. 2019b), excluding the source area (*Zone A*), the volume of the sliding mass is approximately 31.95×10^4 m^3. Additionally, some materials, with a volume of approximately 9.0×10^4 m^3, stopped accumulating near the source area (*Zone A*). Therefore, the total volume of the landslide is estimated to be 40.85×10^4 m^3.

The geological profile 1-1′ after the landslide was drawn through field investigation, aerial image interpretation, and geological analysis, as shown in Fig. 14.

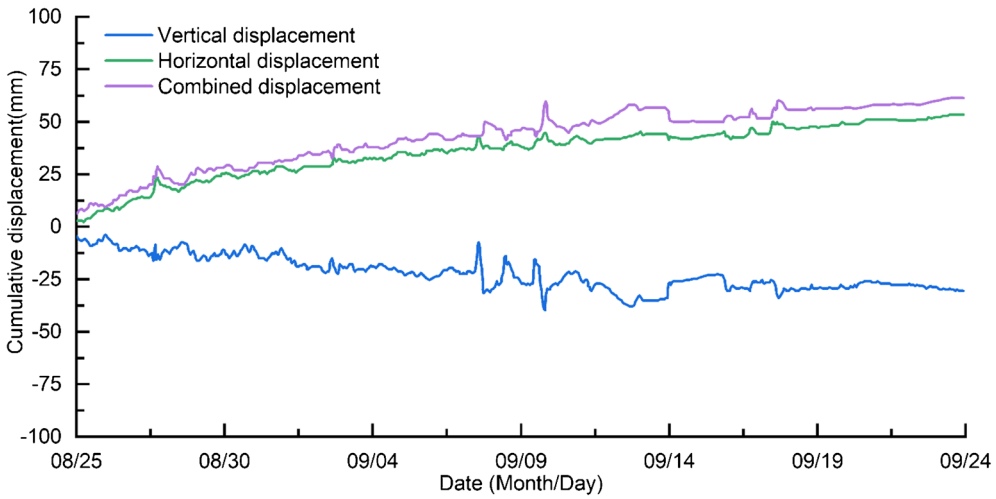

Fig. 12 Displacements in the traction deformation area (*Zone I*) recorded by the BeiDou-based monitoring system

Table 2 Tensile cracks in an impact-traction deformation area (*Zone II-1*)

Crack number	Altitude (m)	Strike angle (°)	Extension length (m)	Maximum width (cm)
C6	998	110	6	10
C7	995	90	40	10
C8	994	70	30	20

Predisposing factors and trigger

The effect of weak interlayers in the Xigeda Formation

The Xigeda Formation is a set of interbeds composed of semi-consolidated silt, fine sand, and clay; thus, this formation is an extremely soft rock with poor engineering properties. The Jinsha River, Yalong River, and Dadu River basins in Southwest China are distributed in a discontinuous strip and sheet shape, with a total area of 4×10^4 km^2 (Zhu and Wu 2008). The siltstone in the Xigeda Formation has weathered to form a loose porous medium with high permeability, which is conducive to surface water infiltration. In the Xigeda Formation, there are thin layers of claystone and carbonaceous claystone intercalations, with a high content of hydrophilic clay minerals such as illite and montmorillonite (Yu et al. 2012). This kind of clay interlayer on a slope is a common potential sliding surface (Rahardjo et al. 2005; Wang et al. 2020). According to field investigation and drilling data, the sliding zone of the Zhonghaicun landslide is composed of thin claystone and carbonaceous claystone with a thickness of 0.1–0.3 m in the completely weathered Xigeda Formation. When they are saturated, these weak intercalations easily soften and eventually become the sliding zone of landslides.

We obtained four soil samples from the source area (*Zone A*) and the impact sliding area (*Zone B*) during the field investigation. Through laboratory tests, the physical and mechanical properties of the samples were obtained, as shown in Table 3. The test results show that the sliding zone soil was nearly saturated, and the natural water content (32.6–33.6%) was close to its liquid limit (34.2–36.2%). Under the rapid direct test condition, the cohesion force of the sample was 12.6–14.9 kPa, and the internal friction

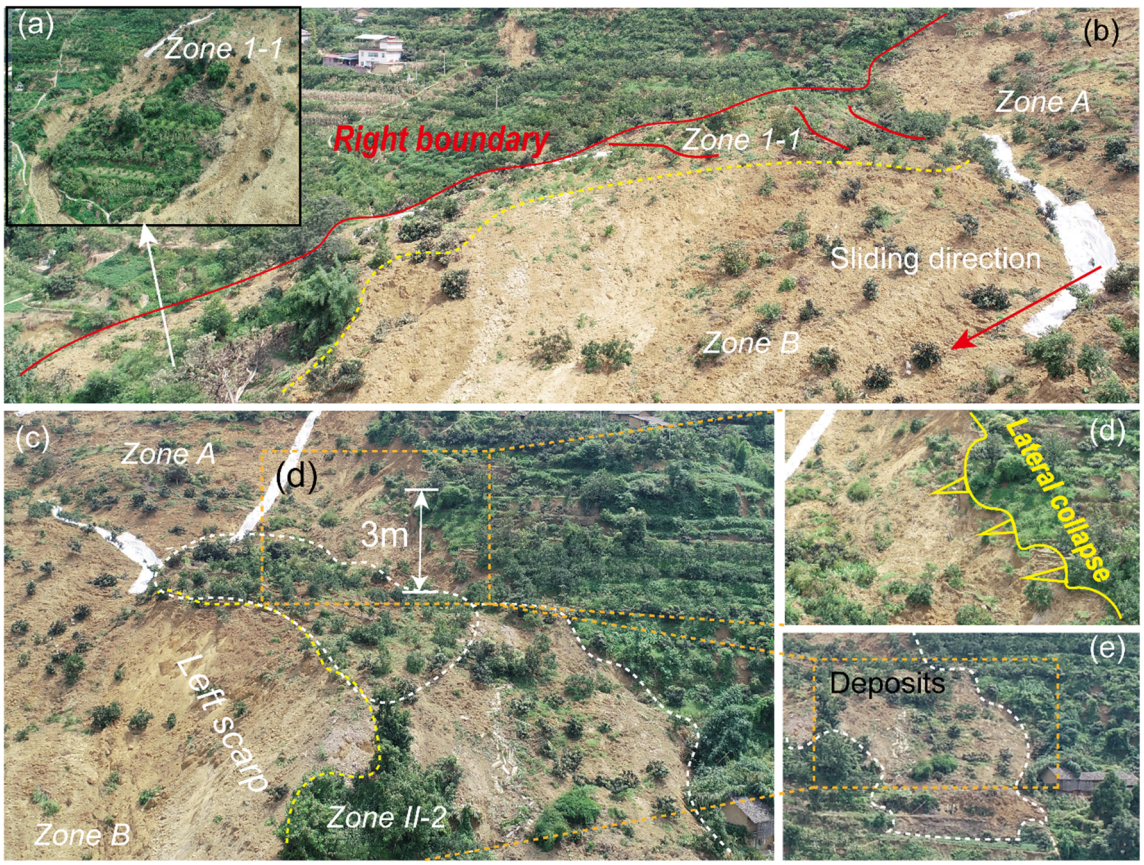

Fig. 13 The impact-traction deformation area (*Zone II*) of the Zhonghaicun landslide: **a**–**b** the impact-traction deformation area (*Zone II-1*) on the right side of the landslide; **a** is located in the lower part and is not covered by landslide deposits, and **b** is located on the upper platform with intense deformation. **c**–**e** The impact-traction deformation area (*Zone II-2*) on the left side of the landslide; **d** is located on the upper platform with intense deformation, and **e** is located at the lower part and covered by landslide debris

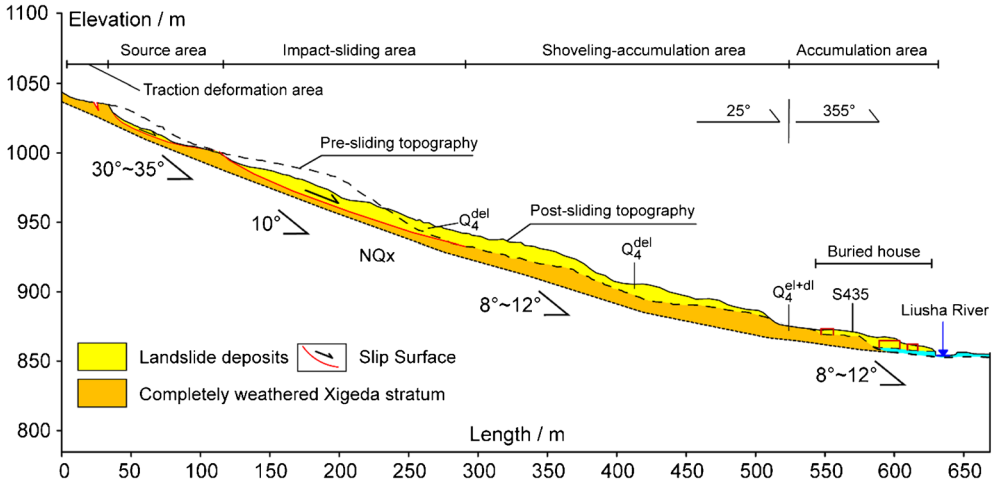

Fig. 14 Post-landslide longitudinal profile 1-1′ in Fig. 6b

angle was 10.8°–11.9°. After continuous rainfall, the increase in water content will weaken the strength of sliding zone soil, which is not conducive to the stability of the landslide.

Persistent rainfall preceding the landslide

Affected by the monsoon climate, the temporal distribution of annual rainfall is uneven, and the rainfall from May to October accounts for 81.2% of the annual rainfall. Over the past 10 years, the average monthly rainfall shows that the rainfall is usually the highest in July. As shown in Fig. 3, since August 2020, the study area has suffered from continuous heavy rainfall, with a cumulative precipitation of 266.1 mm, which is more than the monthly cumulative rainfall in the rainy season in previous years. Interviews of residents showed that there was no rainfall in the landslide area during the 2 days before the landslide occurred (i.e., on the 19th and 20th), but several tension cracks were found in the landslide area. Finally, the landslide lagged behind the rainfall and began to slide in the early morning of August 21.

Continuous rainfall will increase the soil moisture content and the sliding force of the landslide mass and may reduce the stability of the slope. Under the combined action of gravity and rain, the softening contact surface is prone to slip. The connectivity of the potential slip surface increases gradually, and the tensile deformation at the back of the slope also intensifies. Additionally, during and after rainfall, the rainfall seepage process will continue to occur inside the slope (Wu et al. 2020). With the seepage process, the pore water pressure of the potential sliding surface increases gradually, and the equivalent shear strength of the slope decreases (Yang et al. 2020). Finally, under the action of multiple factors, slope deformation accelerates, resulting in the gradual penetration of potential sliding surfaces and landslide disasters (Hungr et al. 2014). From the image before the landslide (Fig. 1a), it can be seen that rainfall in the landslide source area was effectively absorbed and stored by lush vegetation, which increased the rainfall infiltration.

The secondary landslide caused by impact liquefaction

Vibration liquefaction is a typical failure mode of soil structure under vibration load and is extremely harmful to engineering facilities. As a special form of vibration liquefaction, impact liquefaction is the liquefaction of highly saturated soil under impact load (Meng et al. 1999; Zhang and Meng 2003; Rahmani and Naeini 2020). In recent years, impact liquefaction is considered one of the important mechanisms of high-speed and long-distance landslides (Wang et al. 2003; Sassa et al. 2004; Peng et al. 2018; Dun et al. 2020).

The sliding of the source area (*Zone A*) results in many landslide materials impacting the impact sliding area (*Zone B*). Under the impact load, the soil particles' pore channels in the sliding zone become narrower, the original structure of the particles is destroyed, and some low-hardness minerals are broken to form clastic particles. These clastic particles move rapidly under the action of water pressure, blocking some small channels. At this time, the sliding zone soil is completely saturated by the impact,

Table 3 The test results of the physical and mechanical parameters of the landslide sliding surface samples

Sample number	Natural moisture content (%)	Liquid limit (%)	Plastic limit (%)	Saturation (%)	Porosity (%)	Cohesive force (kPa)	Angle of internal friction (°)
SP-1	33.5	35.7	21.2	97	46	12.6	10.8
SP-2	33.6	36.2	21.7	97	46	14.9	11.3
SP-3	33.4	35.8	21.0	97	44	14.8	11.5
SP-4	32.6	34.2	21.2	96	45	14.3	11.9

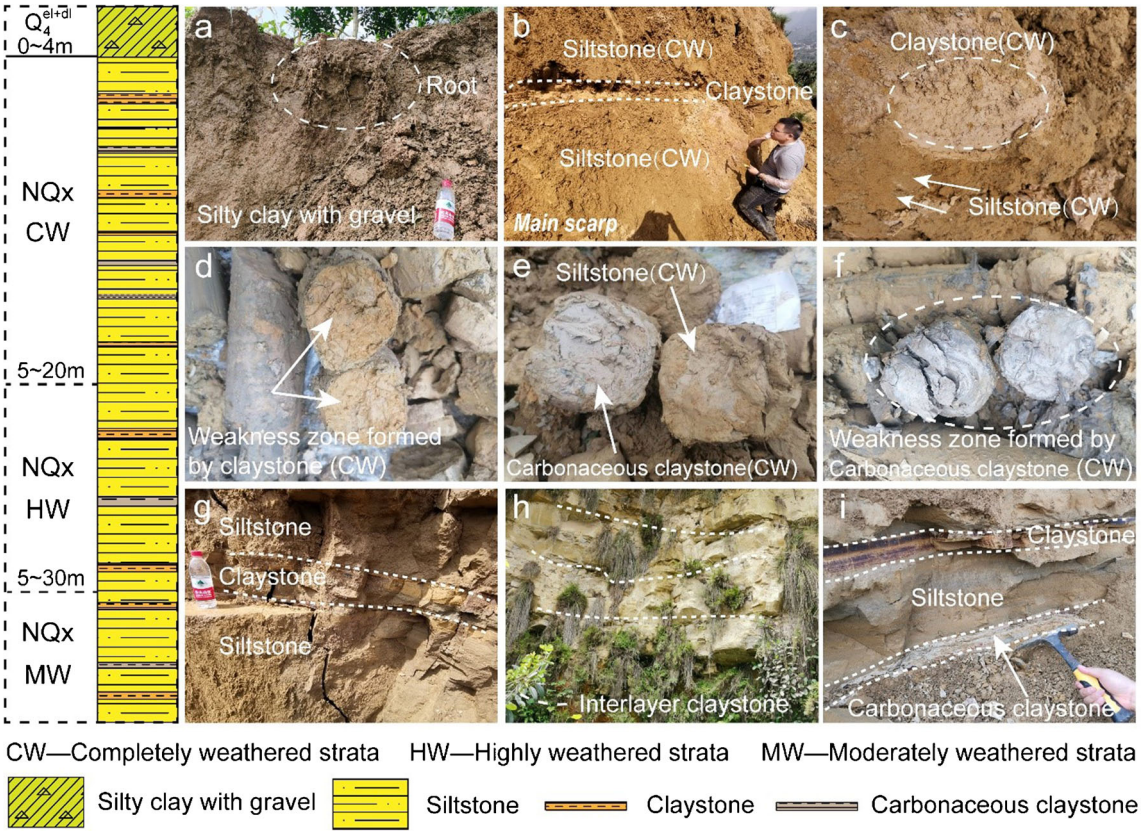

Fig. 15 The distribution characteristics of weak interlayers based on field investigation and borehole data: **a** silty clay of residual slope deposit on the landslide crown; **b**–**c** stratigraphic structure of completely weathered Xigeda Formation discovered by field investigation; **d**–**f** weak interlayers in completely weathered (CW) Xigeda Formation revealed by drilling; **g**–**i** highly weathered (HW) Xigeda formation with weak interlayers; **i** moderately weathered (MW) Xigeda Formation with weak interlayers

and the pore water pressure cannot be quickly dissipated by drainage due to the blockage of the channel. The impact load will sharply increase the total stress and pore water pressure, leading to a rapid decrease in shear strength (Duan et al. 2020). With the rapid decrease in the anti-sliding force and the increase in the sliding force, the sliding surface of the impact sliding area (*Zone B*) penetrates rapidly and slides downward. This fact can be confirmed by the appearance of a flat and smooth sliding surface revealed by field investigation (Figs. 9d and 15c).

Saltatory microrelief of the original slope

Before the landslide, there were four platforms in the original slope area. The microrelief of the scarps between the platforms was developed, which provided good geomorphic conditions for the initiation and movement of the landslide. The original slope of the source area is approximately 30°–35°, and the level-1 platform is located behind the source area, which is conducive to rainwater collection. The level-2 platform blocks the movement of the sliding material in the source area. The rear of the level-3 platform is a

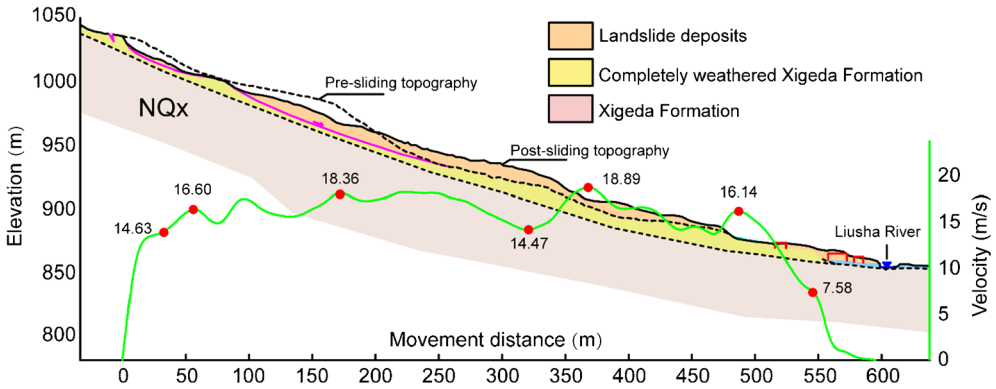

Fig. 16 Estimation velocity of the Zhonghaicun landslide from the 1-1′ profile in Fig. 6b

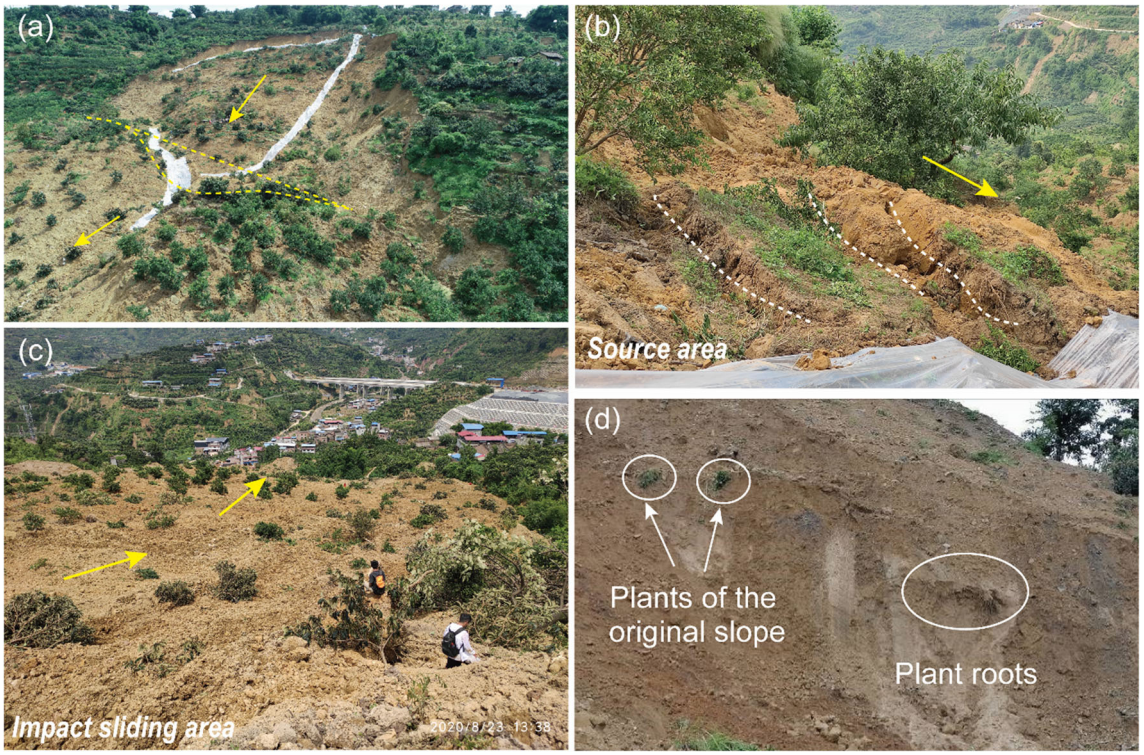

Fig. 17 Field investigation evidence of landslide movement characteristics. **a** wedge-shaped opening in the impact sliding area; **b** the sliding mass in the source area is not completely disintegrated; **c** the sliding mass in the impact sliding area is loose; **d** the original slope in the impact sliding area is covered by sliding mass

scarp landform with a slope of approximately 35°–40°, which provides a free face for the instability of the impact sliding area (*Zone B*). In contrast, the level-3 platform with a gentle slope has accumulated much sliding material and is 7–10 m higher than the original terrain. Multiple houses are built on the level-4 platform, effectively blocking the movement of sliding materials.

The variation in the microrelief in the landslide area will affect the movement speed of the landslide. Figure 16 shows the velocity of the landslide throughout the process of starting, moving, and finally stopping by using the formula proposed by Scheidegger (1973) based on the principle of energy conversion. The results reveal that the velocity of the sliding mass increases rapidly under the action of substantial potential energy when the sliding mass in the source area starts to lose its stability; the velocity of the sliding mass reaches 16.60 m/s soon after sliding out of the rupture surface. Subsequently, as the elevation decreases, the potential energy is transformed into kinetic energy, the velocity increases, and the maximum speed is 18.89 m/s. Then, as the terrain gradually becomes less steep, the debris flow velocity begins to decline sharply until the front of the landslide is finally stopped by the left bank of the Liusha River. The calculation results show that the whole process of landslide movement from the onset to finally stopping lasts for 68 s, and the average speed of the sliding mass during the whole process is as high as 14.3 m/s.

Evolution process of the landslide

Landslides occur as a result of a combination of internal and external factors. External factors, such as slope excavation, underground mining, rainfall, and irrigation, usually play a key role in forming slip zones. The different geological conditions and geomorphic features of the slopes also lead to different failure mechanisms and movement characteristics.

The weathering of the siltstone of the Xigeda Formation in the landslide zone forms highly permeable soil. Simultaneously, the interlayer of thin weathered clay rock in the Xigeda formation has low permeability, facilitating surface water infiltration and groundwater retention. Due to the continuous rainfall, the water content and gravity of the landslide mass increased, which reduced the soil's mechanical properties and were not conducive to the stability of the landslide. The long-term rainfall and seepage action increased the water content and pore water pressure of the sliding zone (Fig. 15), which leads to the expansion of cracks, softening, and strength reduction of the sliding zone (Table 3). In the process, cracks appeared at the back of the slope and expanded further with time (Fig. 5), finally, leading to the first sliding of the upper slope. This fact can be confirmed by the mechanical test data of the soil samples in the sliding surface of the main scarp of the landslide (Table 3) and the slip surface revealed by the inclinometer Z01 (Fig. 8). Moreover, the steep and gentle micro-geomorphology provides good geomorphic conditions for the upper slope failure.

After the sliding of the source area, a part of the sliding mass impacted the critical state slope at the lower part, which led to the rapid penetration of the sliding surface in the impact sliding area and the high-speed downward sliding. The landslide formed a wedge-shaped opening in the middle of the slope (Fig. 17a). The field investigation found that the sliding mass in the source area is not completely disintegrated, and there are many tension cracks on the surface (Fig. 17b). In contrast, the sliding mass in the impact

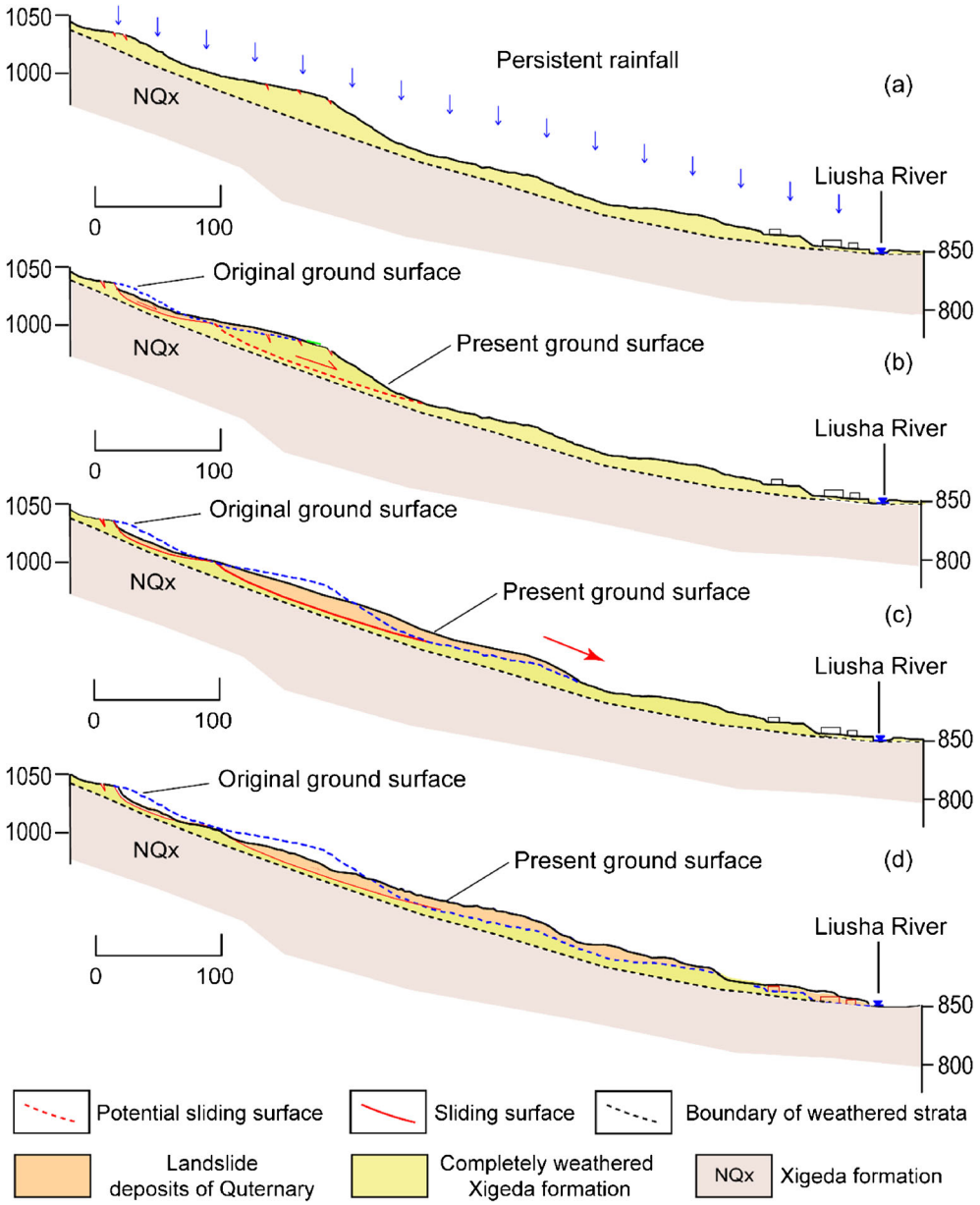

Fig. 18 Conceptual model of the evolution process of the Zhonghaicun landslide: **a** slope deformation stage; **b** sliding and overlay stage; **c** secondary sliding stage; **d** flow-like movement stage

sliding area is loose, and there are no tensile cracks on the slope surface (Fig. 17c). The vegetation between the sliding mass and the initial slope can be seen in the scarp on the left side of the impact sliding area (Fig. 17d). The geomorphic characteristics after the failure reflect the multiple sliding process of the Zhonghaicun landslide. The impact of the first sliding on the lower slope was the main reason for the lower slope sliding. Subsequently, the saturated landslide mass formed long-distance flow-like movement under the action of gravity and impact (Figs. 10 and 11). Finally, affected by the microrelief of the slope and the house, the sliding direction changed (Fig. 10b) and the landslide stopped moving forward (Fig. 11b).

Overall, the Zhonghaicun landslide shows complex triggering mechanisms and movement characteristics. The evolution process of the Zhonghaicun landslide can be understood by comprehensive analysis of geological, geomorphic, meteorological, and other factors. Slope material and microrelief provided the preconditions for the formation of the landslide. Under the condition of continuous rainfall, the effect of water directly led to the occurrence of the landslide. Based on geomorphological and geological surveys, the deformation and failure of the slope mainly experienced four stages: slope deformation, sliding and overlay, secondary sliding, and flow-like movement (Fig. 18):

(1) Slope deformation stage (Fig. 18a). Under the effect of continuous rainfall, rainfall infiltration increased the

saturated bulk density of the sliding mass. The rainwater seeped into the weak interlayer of the slope, causing its shear strength to decrease. Over time, tensile stress areas appeared on the slope under gravity, and tensile cracks appeared on the surface.

(2) Sliding and overlay stage (Fig. 18b). After the rain stopped, the seepage process in the slope continued. With the further deepening of the cracks and the penetration of the sliding surface, the upper slope was damaged, and a large number of landslide materials were loaded on the lower slope in a short time.

(3) Secondary sliding stage (Fig. 18c). Saturated by the upper landslide, the weight of the lower slope increased and the strength of the saturated sliding zone decreased rapidly under the impact, forming a shear sliding surface through the weak interlayer surface, which led to the instability of the impact sliding area.

(4) Flow-like movement stage (Fig. 18d). A part of the sliding mass continued to move downward to form a debris flow. In this process, the original soil of the slope was scraped along the sliding path. Because of the buffer of the gentle slope platform and the blocking of houses, the debris flow slowed down due to the loss of kinetic energy until it moved to the front of the Liusha River.>

Conclusions

The geological background, characteristics, and inducing factors of the Zhonghaicun landslide in Hanyuan County, Sichuan Province, are described. The failure mechanism and evolution process of the landslide are analyzed. According to the elevation ranges and characteristics of the Zhonghaicun landslide, the landslide is divided into seven areas. The research shows that the landslide exhibited a complex movement process. The source area first slid along the weak interlayers and impacted the lower slope, causing secondary sliding. The landslide debris then moves to the toe of the slope at high speed, causing seven people to die and two people to go missing.

The deformation and failure of the Zhonghaicun landslide were related to lithology, geomorphology, and previous rainfall. The high permeability stratum and the weak interlayer were the material basis of the landslide. The steep and gentle slope changes provide favorable geomorphological conditions for rainwater accumulation and landslide movement. Moreover, the previous rainfall increased the pore water pressure of the landslide mass and reduced the mechanical strength of the weak interlayers, which was the main trigger of the landslide.

Acknowledgements

We are very grateful to the Sichuan Institute of Geological Engineering Investigation Group Co. Ltd. for providing borehole data and geotechnical exploration reports. We also grateful for the DOMs and DEMs provided by the 606 Brigade of Sichuan Metallurgical Geological Survey Bureau. The authors also thank the Hanyuan County Meteorological Bureau for providing rainfall data. We would like to thank our team Weikong Zeng, Jinnan Han, and Jiawei Dun, in the College of Environment and Civil Engineering, for cooperating during site investigation and laboratory testing for samples taken from the Zhonghaicun landslide. We also thank the anonymous referees and the editor for their constructive feedbacks and suggestions that encourage us to improve the quality of this paper.

Funding

This research was funded by the National Natural Science Foundation of China (Grant Nos. 41977252, U2005205) and the State Key Laboratory of Geohazard Prevention and Geoenvironment Protection Independent Research Project (Grant No. SKLGP2020Z001).

References

Bezak N, Jež J, Sodnik J, Jemec Auflič M, Mikoš M (2020) An extreme May 2018 debris flood case study in northern Slovenia: analysis, modelling, and mitigation. Landslides 17:2373–2383. https://doi.org/10.1007/s10346-019-01325-1

Bhardwaj A, Wasson RJ, Ziegler AD, Chow WTL, Sundriyal YP (2019) Characteristics of rain-induced landslides in the Indian Himalaya: a case study of the Mandakini Catchment during the 2013 flood. Geomorphology 330(APR.1):100–115. https://doi.org/10.1016/j.geomorph.2019.01.010

Duan Z, Dong C, Zheng W, Tang H, Ma J (2020) liquefaction mechanism of terrace sandy silt under landslide impact. J Eng Geol 28(6):1362–1371. https://doi.org/10.13544/j.cnki.jeg.2019-491

Emanuel K (2005) Increasing destructiveness of tropical cyclones over the past 30 years. Nature 436(7051):686–688. https://doi.org/10.1038/nature03906

Fan L, Lehmann P, McArdell B et al (2017a) Linking rainfall-induced landslides with debris flows runout patterns towards catchment scale hazard assessment. Geomorphology 280(MAR.1):1–15. https://doi.org/10.1016/j.geomorph.2016.10.007

Fan X, Xu Q, Scaringi G, Dai L, Li W, Dong X, Zhu X, Pei X, Dai K, Havenith HB (2017b) Failure mechanism and kinematics of the deadly June 24 2017 Xinmo landslide, Maoxian, Sichuan, China. Landslides 14(6):2129–2146. https://doi.org/10.1007/s10346-017-0907-7

Geertsema M, Hungr O, Schwab JW, Evans SG (2006) A large rockslide–debris avalanche in cohesive soil at Pink Mountain, northeastern British Columbia, Canada. Eng Geol 83(1-3):64–75. https://doi.org/10.1016/j.enggeo.2005.06.025

Geological Bureau of Sichuan Province (1971) Yingjing Geological Map (1:200000). Map No. H-48-XIX. (In Chinese)

Guzzetti F, Peruccacci S, Rossi M, Stark CP (2007) Rainfall thresholds for the initiation of landslides in central and southern Europe. Meteorog Atmos Phys 98(3):239–267. https://doi.org/10.1007/s00703-007-0262-7

He K, Liu B, Hu X (2020) Preliminary reports of a catastrophic landslide occurred on August 21, 2020, in Hanyuan County, Sichuan Province, China. Landslides. https://doi.org/10.1007/s10346-020-01566-5

Hungr O, Leroueil S, Picarelli L (2014) The Varnes classification of landslide types, an update. Landslides 11(2):167–194. https://doi.org/10.1007/s10346-013-0436-y

Kotlyakov VM, Rototaeva OV, Nosenko GA (2004) The September 2002 Kolka glacier catastrophe in North Ossetia, Russian Federation: evidence and analysis. Mt Res Dev 24(1):78–83. https://doi.org/10.1659/0276-4741(2004)024[0078:TSKGCI]2.0.CO;2

Li Y, Ma C, Wang Y (2019) Landslides and debris flows caused by an extreme rainstorm on July 21 2012 in mountains near Beijing, China. B Eng Geol Environ 78(2):1265–1280. https://doi.org/10.1007/s10064-017-1187-0

Ma P, Peng J, Wang Q, Zhuang J, Zhang F (2019a) The mechanisms of a loess landslide triggered by diversion-based irrigation: a case study of the South Jingyang Platform, China. B Eng Geol Environ 78(7):4945–4963. https://doi.org/10.1007/s10064-019-01467-5

Ma S, Xu C, Xu X (2019b) Volume expansion rates of seismic landslides and influencing factors: a case study of the 2008 Wenchuan earthquake. J Mt Sci-Engl 16(8):1731–1742. https://doi.org/10.1007/s11629-019-5479-7

Meng XY, Zhang JF, Yu SB et al (1999) The variation of porewater pressure and its relationship with liquefaction and densification in saturated sand under impact loading. Chin J Geotech Eng 03:7–11

Peng JB, Ma PH, Wang QY et al (2018) Interaction between landsliding materials and the underlying erodible bed in a loess flowslide. Eng Geol 01:38–49. https://doi.org/10.1016/j.enggeo.2018.01.001

Rahardjo H, Lee TT, Leong EC, Rezaur RB (2005) Response of a residual soil slope to rainfall. Can Geotech J 42(2):340–351. https://doi.org/10.1139/t04-101
Rahmani H, Naeini SA (2020) Influence of non-plastic fine on static iquefaction and undrained monotonic behavior of sandy gravel. Eng Geol 275:105729. https://doi.org/10.1016/j.enggeo.2020.105729
Sassa K, Wang G, Fukuoka H, Wang F, Ochiai T, Sugiyama M, Sekiguchi T (2004) Landslide risk evaluation and hazard zoning for rapid and long-travel landslides in urban development areas. Landslides 1:221–235. https://doi.org/10.1007/s10346-004-0028-y
Scheidegger AE (1973) On the prediction of the reach and velocity of catastrophic landslides. Rock Mech 5(4):231–236. https://doi.org/10.1007/BF01301796
Shrestha S, Kang T (2019) Assessment of seismically-induced landslide susceptibility after the 2015 Gorkha earthquake, Nepal. B Eng Geol Environ 78(3):1829–1842. https://doi.org/10.1007/s10064-017-1191-4
Tang H, Wasowski J, Juang CH (2019) Geohazards in the three Gorges Reservoir Area, China — lessons learned from decades of research. Eng Geol 261:105267. https://doi.org/10.1016/j.enggeo.2019.105267
Wang G, Sassa K, Fukuoka H (2003) Downslope volume enlargement of a debris slide-debris flow in the 1999 Hiroshima, Japan, rainstorm. Eng Geol 69(3-4):309–330. https://doi.org/10.1016/S0013-7952(02)00289-2
Wang J, Xiao L, Zhang J, Zhu Y (2020) Deformation characteristics and failure mechanisms of a rainfall-induced complex landslide in Wanzhou County, Three Gorges Reservoir, China. Landslides 17:419–431. https://doi.org/10.1007/s10346-019-01317-1
Wu L, Huang R, Li X (2020) Hydro-mechanical analysis of rainfall-induced landslides. Springer, Singapore. https://doi.org/10.1007/978-981-15-0761-8_3
Xu C, Xu X, Shen L, Yao Q, Tan X, Kang W, Ma S, Wu X, Cai J, Gao M, Li K (2016) Optimized volume models of earthquake-triggered landslides. Sci Rep 6(1):29797. https://doi.org/10.1038/srep29797
Yang S, Su L, Zhang C, Li C, Hu l (2020) Analysis of seepage characteristics and stability of Xigada Formation slope under heavy rainfall. J Civil Environ Eng 42(4):19–27. https://doi.org/10.11835/j.issn.2096-6717.2020.024
Yin Y, Wang H, Gao Y, Li X (2010) Real-time monitoring and early warning of landslides at relocated Wushan Town, the Three Gorges Reservoir, China. Landslides 7(3):339–349. https://doi.org/10.1007/s10346-010-0220-1
Yin Y, Zheng W, Li X, Sun P, Li B (2011) Catastrophic landslides associated with the M8.0 Wenchuan earthquake. B Eng Geol Environ 70(1):15–32. https://doi.org/10.1007/s10064-010-0334-7
Yu H, Li C, Zhou J, Chen W, Long J, Wang X, Peng T (2020) Recent rainfall- and excavation-induced bedding rockslide occurring on October 22 2018 along the Jian-En expressway, Hubei, China. Landslides 17:2619–2629. https://doi.org/10.1007/s10346-020-01468-6
Yu X, Xiong Q, Song Y, He C (2012) Preliminary analysis on the characteristics of slide-prone strata of Xigeda formation in Hanyuan County, Sichuan Province. Res Environ Eng 26(B04):36–38. https://doi.org/10.3969/j.issn.1671-1211.2012.z1.009
Zhang F, Liu G, Chen W, Liang S, Chen R, Han W (2012) Human-induced landslide on a high cut slope: a case of repeated failures due to multi-excavation. J Rock Mech Geotech Eng 4(4):367–374. https://doi.org/10.3724/SP.J.1235.2012.00367
Zhang J F, Meng X Y (2003) Build-up and dissipation of excess pore water pressure in saturated sand under impact loading. Chin J Rock Mech Eng, (9): 1463–1468.
Zhu B, Wu X (2008) An analysis of rainfall-induced landslide in colluvial and eluvial soils overlying Xigeda strata, Southwestern Sichuan, China. J Eng Geol 16(Suppl.): 487–494.

X. Yi · W. Feng (✉) · H. Bai · H. Shen
State Key Laboratory of Geohazard Prevention and Geoenvironment Protection,
Chengdu University of Technology,
Chengdu, 610059, Sichuan, China
Email: fengwenkai@cdut.cn

X. Yi
e-mail: xiaou@stu.cdut.edu.cn

H. Li
Sichuan Academy of Territorial Space Ecorestoration and Geohazard Prevention,
Chengdu, 610081, Sichuan, China